

Atomistic simulation of doping effects on growth and charge transport in Si/Ag interfaces in high-performance solar cells

Keith T. Butler and John H. Harding

Department of Materials Science and Engineering, University of Sheffield, Mappin Street, Sheffield S1 3JD, United Kingdom

(Received 4 July 2012; published 21 December 2012)

We present the results of a first-principles atomistic simulation study of the effects of phosphorus doping on the silver/silicon interface as found in high-performance solar cells. Calculating the interfacial stabilities of the (110)/(110) and (111)/(111) interfaces we demonstrate how the presence of phosphorus increases the nucleation rate of silver crystallites and how the relative stabilities of the interfaces depend on the doping. We then calculate the electronic structure of the interfaces, demonstrating how the presence of phosphorus leads to a buildup of positive charge in the silicon and an opposite negative charge in the silver. Finally we show how this charge buildup significantly affects the n -type Schottky barriers at the interfaces, in both cases lowering the Schottky barrier by more than 100 meV.

DOI: [10.1103/PhysRevB.86.245319](https://doi.org/10.1103/PhysRevB.86.245319)

PACS number(s): 73.30.+y, 88.40.jj, 71.15.Mb, 61.72.uf

I. INTRODUCTION

The silicon silver (Si/Ag) interface plays an important role in modern industrial high-performance solar cells, in which Ag is commonly used as a contact for the n -type Si emitter.^{1,2} The contact resistance (R_c) at this interface plays a significant role in determining the overall device efficiency; indeed the majority of process-induced losses in industrial crystalline silicon (c -Si) solar cells can be attributed to the formation of metal-semiconductor contacts. Recently a number of studies have investigated the mechanisms of both contact formation^{3,4} and charge transport⁵ at this interface.

In this paper we investigate the role of phosphorus doping on R_c using *ab initio* simulations and building on previous results for undoped Si/Ag interfaces identified in c -Si solar cells.⁶ Currently industrially produced solar cells require high surface concentrations of P, exceeding the solubility limit in Si, to achieve ohmic contacting. This situation is undesirable as the high surface concentration of P results in recombination losses, which in turn lead to current and voltage losses. We consider two major roles played by P, first in promoting the formation of Si/Ag interfaces, second by altering the charge transport barrier at the Si/Ag interfaces formed.

The Si/Ag interface in high-performance solar cells has been the subject of significant amounts of research. Ballif *et al.*^{1,7} used high-resolution electron microscopy (HREM) and energy-dispersive spectroscopy (EDS) to investigate the interface, demonstrating that the interface is composed of nanoscale Ag crystallites growing into the Si wafer. Such pyramidal crystallites have also been reported for other metal-semiconductor interface systems, for example Cu-Si⁸ and Al-Si.⁹

The performance of the solar cell depends on sufficient contact area being established between the Si and Ag, so increasing the number and size of Ag crystallites is desirable. Schübert¹⁰ has reported systematic studies of the effect of P surface concentration and temperature on the Ag crystallite formation. This study showed an increased number and size of crystallites with increased doping and temperature and concludes that in highly doped emitters “the activation energy for initiating Ag crystal growth on silicon can be assumed to

be lower”. In addition Schübert demonstrated the effect of Si wafer texturing on the crystallite growth, concluding that the activation energy for crystal growth is also dependent on Si crystal orientation. In this paper, using *ab initio* techniques to calculate the thermodynamic work of separation for Si/Ag interfaces and its dependence on doping and orientation, we are able to explain these results within the context of classical nucleation theory (CNT). It is important that we stress, from the outset, the fact that CNT can provide, at best, semiquantitative results. Therefore, while the results which we present here should be treated as an explanation of the phenomenon of increased Ag crystallite formation in the presence of P doping, they should not be treated as a quantitative prediction of the degree to which crystallization is increased by the presence of P doping. Such predictions require a further set of careful calculations, which are beyond the scope of the current study.

In addition to increasing the contact area between Si and Ag it is desirable to reduce the contact resistivity (ρ_c). ρ_c is exponentially dependent on the Schottky barrier height (SBH).^{11,12} Basic Schottky theory suggests that the SBH at an interface should be dependent only on the bulk properties of the two materials at the interface, the work function of the metal, and the electronegativity of the semiconductor.^{13,14} However there have been many examples, both theoretical and experimental, showing the influence of the interface itself on the SBH.^{15–18} In fact the SBH can be partitioned into two terms (SBH = $\Delta E_V + \Delta V$).¹⁹ ΔE_V depends on the relevant valence band edges in the two materials and is characteristic of the bulk materials, while ΔV is the electrostatic potential lineup at the interface, and can, in principle, depend on the local structure.

We have previously demonstrated that the SBH at the pure Si/Ag interface can depend on the crystal orientation of the interface.⁶ In this paper we extend this study to account for the effects of P doping to simulate the Ag interface with an n -type emitter. We demonstrate the lowering of the SBH in the presence of P doping. The values calculated in this study are necessary as input parameters for macroscopic device models. In conjunction with our findings relating to the effects of P on

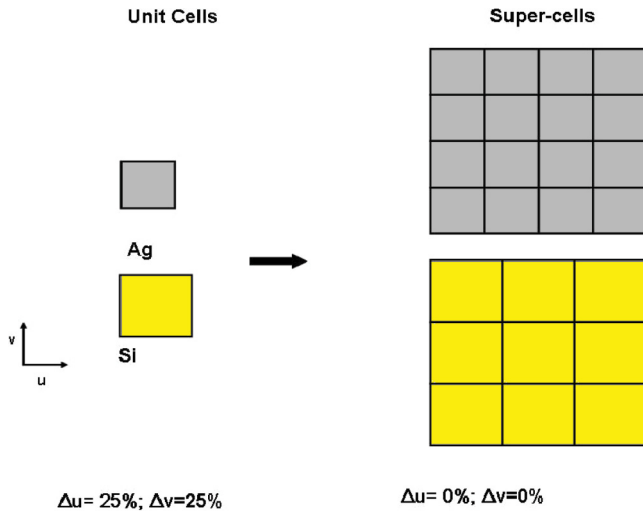


FIG. 1. (Color online) Schematic illustration of the use of supercells to overcome lattice mismatch. Left: Si ($u = 7.679 \text{ \AA}$, $v = 7.679 \text{ \AA}$) and Ag ($u = 5.784 \text{ \AA}$, $v = 5.784 \text{ \AA}$) unit cells differ by 25% in u and v lattice directions. Right: Si ($\times 3$) and Ag ($\times 4$) supercells have very little lattice mismatch.

the crystallization of Ag these values can be used to inform future cell fabrication design.

II. NUMERICAL METHODS

All starting geometries for the current simulations were taken from previous work on the undoped Si/Ag interface.⁶ All density functional theory (DFT) calculations were performed using the Vienna *Ab initio* Simulation Package (VASP).²⁰ In all cases we employed the PBE functional²¹ with a plane wave cutoff of 450 eV and projector augmented wave pseudopotentials.²² All supercells in this paper consist of various numbers of Si and Ag unit cells in the plane of the interface, chosen in order to minimize the effects of lattice mismatch, as illustrated in Fig. 1. In all cases the remaining lattice mismatch, which was 0.3%, was accounted for by compression of the Ag. To investigate the effect of different doping levels we have used supercells with different numbers of Si atoms. The compositions and doping levels of all cells used in this paper are presented in Table I. We have investigated the (110)/(110) and (111)/(111) interfaces, which we have previously identified by transition electron microscopy⁶ and which constitute the faces of crystallites growing into the (111)

TABLE I. Supercell setups for the interface calculations, showing the number of periodic images of each material used in the setup in order to reduce minimize lattice mismatch and alter the doping concentrations. P doping concentrations are also included.

Interface	Ag ($u \times v$)	Si ($u \times v$)	N_D (cm^{-3})
Ag(110)/Si(110)	4×4	3×3	
Ag(110)/Si(110)	8×4	6×3	1.73×10^{20}
Ag(110)/Si(110)	12×4	9×3	1.16×10^{20}
Ag(111)/Si(111)	4×4	3×3	
Ag(111)/Si(111)	8×4	6×3	2.78×10^{20}
Ag(111)/Si(111)	16×4	12×3	1.39×10^{20}

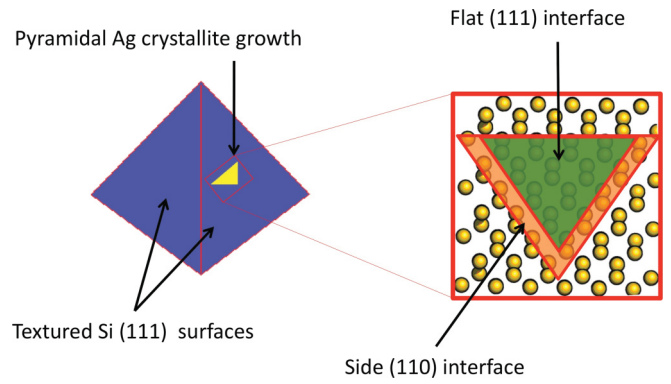


FIG. 2. (Color online) Schematic illustration of the growth habits of Ag crystallites on flat textured Si (111) surface. The crystallite grows in a pyramidal shape with (110) planes on the side and a (111) plane at the base.

face of textured c-Si, as found in many high-performance solar cells. The geometry of these crystallites is illustrated in Fig. 2.

III. DOPING ENERGY AND LATTICE STRAIN

The first step in our investigation of the effects of P doping at the Si/Ag interface is to establish the preferred location of P dopant atoms at the interface for the various configurations. It is well known that P dopes Si substitutionally,^{23,24} so our method involves replacing a Si atom in each atomic layer moving away from the interface one at a time and calculating the resultant supercell energy. The energy of substituting a Si atom with a P atom, relative to the energy of substitution on the bulk Si, is calculated from

$$E = E_{\text{Doped}}^{\text{Interface}} - E_{\text{Doped}}^{\text{Bulk}} + E_{\text{Pure}}^{\text{Bulk}} - E_{\text{Pure}}^{\text{Interface}}. \quad (1)$$

Applying this formula we obtain the doping energies presented in Fig. 3. This shows a clear trend at both interfaces for the segregation of P away from the bulk Si and towards the interface. However there is a notable difference, in that the dopant atom at the 110 interface prefers to sit one atomic layer back from the interface, while at the 111 interface the preferred position is at the interface itself. Since the most favorable sites for substitution are found to be the first layer in the (111)/(111) interface and the second layer in the (110)/(110) interface, all studies of the effect of doping from here on in this study will be based on these substitution sites.

In Fig. 3 we present the distortions to the atomic positions at the interfaces, both with and without doping. This figure presents the root-mean-squared displacements (RMSD) of the atoms in the supercell from their idealized lattice positions. At both interfaces the majority of the strain caused by the formation of an interface from bulk materials is manifested in the Ag side of the interface. At both interfaces the strain penetrates further into the Ag lattice in the absence of a doping P atom. This effect is particularly notable at the 110 interface. Interestingly the presence of the dopant atom does not seem to cause any major strain on the Si lattice at the (111)/(111) interface, beyond that caused by the formation of the interface. Clearly in the case of the doped (110)/(110) interface the RMSD variations in the Si layer are not monotonic away from the interface. This is due to the fact that the dopant P

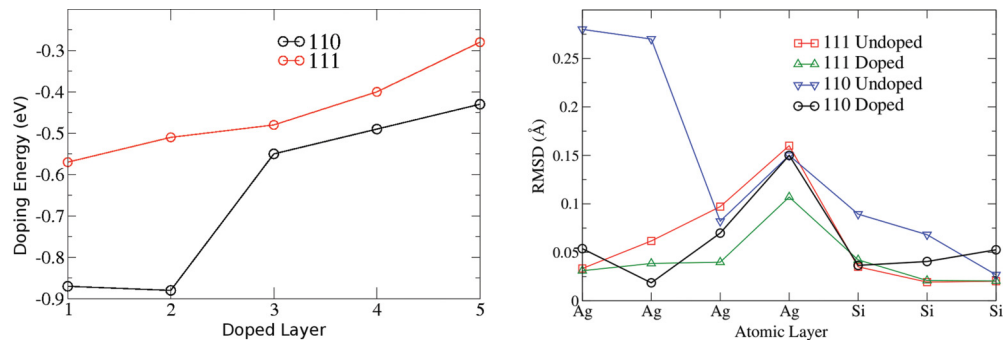


FIG. 3. (Color online) Left: Relative energy of doping with respect to the layer in which Si is replaced. Values are relative to the most stable doping layer. The layers are counted beginning at the interface. Right: RMSD of the Si and Ag atoms in the layers closest to the interface from ideal crystal position upon formation of the interface.

atom is present in the second layer away from the interface and introduces larger local distortions in the second and third layers of Si than the interface introduces in the first layer.

IV. INTERFACE ENERGY AND CRYSTALLITE NUCLEATION

In order to consider the possible mechanisms leading to the promotion of Ag crystallite formation in the presence of P doping we now examine the energies associated with the various interfaces both in the presence and absence of P. The possibility we consider is that P lowers the interfacial energy thereby promoting nucleation of Ag at the Si interface during the firing process. According to classical nucleation theory (CNT),²⁵ the energy barrier for homogeneous nucleation is given by

$$\Delta G_{\text{Homo}} = \frac{16\pi\sigma^3}{3(G_v)^2}, \quad (2)$$

where σ is the surface energy and G_v is the bulk free energy difference between the phases.

In the case of nucleation at a heterointerface the free energy barrier to nucleation is modified by a factor depending on the interfacial free energies between the phases present. The relationships between the free energies can in turn be related to the contact angle formed by a droplet of the liquid phase on the solid phase:²⁶

$$\Delta G_{\text{Hetero}} = \Delta G_{\text{Homo}} \times f(\theta), \quad (3)$$

where $f(\theta) = \frac{1}{2} - \frac{3}{4} \cos(\theta) + \frac{1}{4} \cos^3(\theta)$ is a function of the wetting angle of material B on the surface of material A. The wetting angle can be related to a thermodynamic quantity known as the work of adhesion (F_{ad}),²⁷ which is the reversible free energy of forming two free surfaces from an interface, from the formula

$$F_{ad} = \sigma_{1v}[1 + \cos(\theta)], \quad (4)$$

with σ_{1v} the interfacial energy of the liquid silver with the glass medium present during the firing process, and θ the wetting angle.

However, from a theoretical point the direct calculation of F_{ad} presents some serious problems, as it includes all possible changes due to factors such as diffusion, plastic, and elastic deformation. Figure 4, adapted from the paper of Finnis,²⁷

to which we refer the reader for a fuller explanation of this topic, presents the relationship between F_{ad} and a property known as the work of separation (W_{sep}), which is a much more tractable quantity to obtain from simulations. Figure 4 shows that F_{ad} is W_{sep} minus the energy changes arising from diffusive relaxation and both elastic and plastic deformation of the new interfaces created by removing the silver from the silicon. If we therefore have two systems in which the energies of diffusion and elastic and plastic deformation are equal, the relative values of W_{sep} would provide the relative values of F_{ad} . In this study we compare only Si surfaces with the same crystallographic orientation; therefore the trends in the W_{sep} should reflect the trends in F_{ad} in a semiquantitative fashion. To go beyond this and compare rates for the different Si surfaces would require the explicit calculation of F_{ad} , since the deformation and diffusion energies at the different Si surfaces would be expected to differ, and is beyond the scope of this study.

We note that accurate quantitative calculation of the energy of doping would also require some accounting for the finite cell size effects introduced by the use of periodic boundary conditions. The effects of interactions between defects across cell boundaries can be accounted for *a priori*, by methods such as the local moment countercharge method,²⁸ or by extrapolation of the results to the limit of infinite cell size.^{29,30}

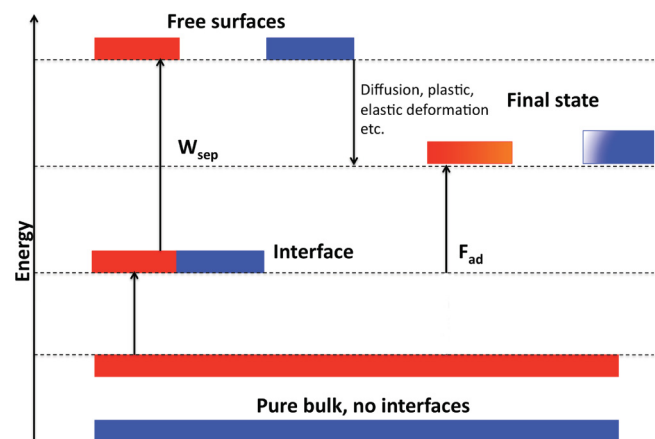


FIG. 4. (Color online) Schematic representation of the relationship between F_{ad} and W_{sep} . Adapted from Ref. 27.

TABLE II. Calculated works of separation for the doped and undoped Si/Ag interfaces.

Interface	W_{sep} (J m ⁻²)		ΔW_{sep} (J m ⁻²)
	Doped	Undoped	
(110)/(110)	0.99	1.90	0.91
(111)/(111)	1.28	1.47	0.19

The finite cell effects are of most importance when the defects carry strongly localized point charges and the relaxations in the lattice around the defect are large;³¹ neither of these is the case in our systems. The W_{sep} energies are calculated for the largest supercells in this study, which includes up to third-nearest-neighbor atoms within the same periodic image as the dopant atom. Given that the results we present here are semiquantitative at best and are intended to explain, rather than quantify, the effects of P doping on Ag crystallite formation, we feel that the use of such a large supercell without application of corrections is sufficient, while noting that for further predictive studies such corrections would be required.

In our system we have the complication that the silicon and silver are in contact with a glass, rather than a vapor. Thus, in order to consider the nucleation rates at the different crystallographic orientations we would require the interface energy between the interfaces and the glass medium. Given the necessity for computationally demanding techniques when calculating interface free energies of liquid/solid interfaces,^{32,33} this task is beyond the scope of the current study. Rather, we consider the crystallographic orientations separately. This allows us to make a semiquantitative comparison between the doped and undoped interface nucleation rates for a given interface within CNT.

The calculated values for W_{sep} in the presence and absence of P doping are presented in Table II. This clearly demonstrates that P doping increases W_{sep} , implying more stable interfaces and larger values of $\cos(\theta)$ and hence a greater reduction of the energy barrier to nucleation. This can be directly related to the result from the section on doping energy and lattice strain where we demonstrated the decreased strain in the Ag lattice in the presence of P doping. To illustrate how this changing of the interface stability alters the number of crystallites formed we consider the nucleation rate (I) from CNT, given by

$$I = \beta N \exp \left[\frac{-\Delta G_{\text{Hetero}}}{k_B T} \right], \quad (5)$$

where N is the number of potential nucleation sites per unit volume, T is temperature, k_B is Boltzmann's constant, and β is the rate of diffusion of molecules to the cluster. We calculate the wetting angle by substituting W_{sep} for F_{ad} in Eq. (4). This means that our results must be treated as at best semiquantitative; however, given the almost pure nature of both materials in our system this approximation is reasonable to make. We use this value to calculate an energy barrier relative to the barrier for Ag homogenous nucleation from Eq. (3). We can then consider the rate of nucleation in the doped relative

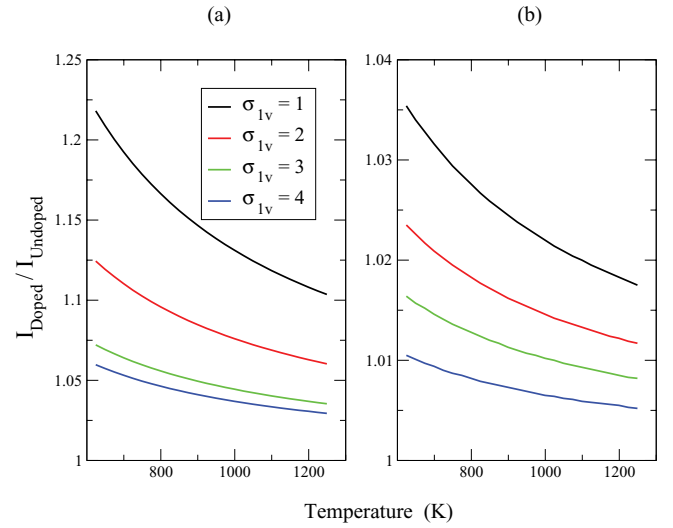


FIG. 5. (Color online) The ratio of nucleation rates for a range of Ag/glass interfacial energies (σ_{lv}) at the doped and undoped interfaces for the (111)/(111) Si/Ag interface (left) and the (110)/(110) Si/Ag interface (right).

to the undoped case from

$$\frac{I_{\text{Doped}}}{I_{\text{Undoped}}} = \exp \left[\frac{\Delta G_{\text{Hetero}} [f(\theta)_{\text{Undoped}} - f(\theta)_{\text{Doped}}]}{k_B T} \right]. \quad (6)$$

From Eq. (4), it is clear that the $\cos(\theta)$ will depend on the value of the silver/glass interface tension, as well as F_{ad} . Thus the nature of the glass will influence the manner in which doping affects the barrier to nucleation. In order to illustrate how the nucleation rate is increased by the presence of P doping, and how this increase in turn depends on the temperature and the silver/glass interface tension, we have plotted the ratio of nucleation rate in the presence of P relative to the rate on pure Si for the two interfaces in Fig. 5.

The normalized nucleation rates are presented in Fig. 5, which shows the ratio of nucleation rates for the doped and undoped systems for the (111)/(111) Si/Ag interface (left) and the (110)/(110) Si/Ag interface (right). Clearly the nucleation rate is increased for both interfaces when doping is present, with a significantly more pronounced effect at the 111 interface. This result explains the increased density of Ag crystallites observed in the presence of higher P doping of Si crystals.¹⁰

V. CHARGE REARRANGEMENTS

To get a clear picture of the charge distributions across our interfaces we consider first the planar average of the potential in the plane (area S) orthogonal to the interface:¹⁹

$$\bar{n}(z) = \frac{1}{S} \int_S n(x, y, z) dx dy. \quad (7)$$

This yields a one-dimensional charge density [$\bar{n}(z)$] from the three-dimensional density [$n(x, y, z)$]. We consider the difference in charge density at the interfaces compared to the undoped cases by subtracting the densities. The results of these calculations are presented in Fig. 6. These plots show

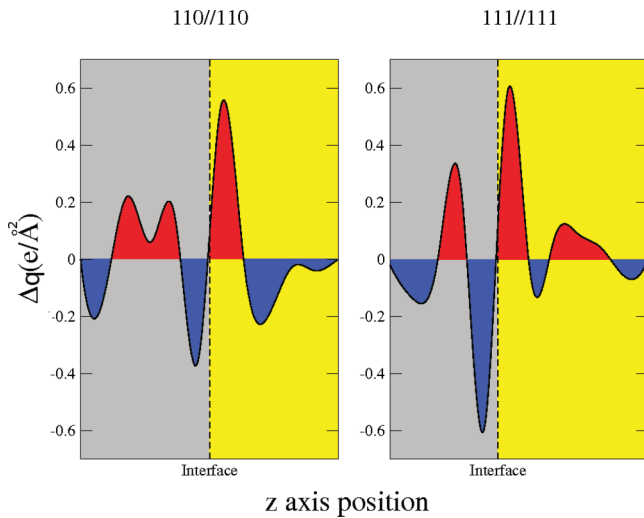


FIG. 6. (Color online) Charge rearrangements after doping the Si/Ag (110) and (111) interfaces. The graph shows the linear average of charge density in the direction orthogonal to the interface in the doped system minus that in the undoped system. Grey section is the silver layer; yellow section is the silicon layer.

the change in the number of excess electrons upon doping the system. Clearly in both cases there is an increase in the electron density at the semiconductor side of the interface, with a complementary decrease in the electron density at the metal side of the interface. The effect is larger in the (111)/(111) interface, which we showed in a previous study⁶ has no charge transfer in the undoped system. This result can have implications for the charge transport barrier at this interface. The charge at the interface due to this charge transfer results in a dipole forming at the interface; in effect the semiconductor has a partially ionic termination. As has been shown¹⁶ the positive charge at the semiconductor surface lowers the potential in the semiconductor and decreases the *n*-SBH. We will now consider the Schottky barriers at the interfaces to demonstrate the effect of this charge.

VI. ELECTRONIC STRUCTURE AND SCHOTTKY BARRIERS

The projected densities of states (PDOS) for the system across the interface are presented in Fig. 7. As we found in the

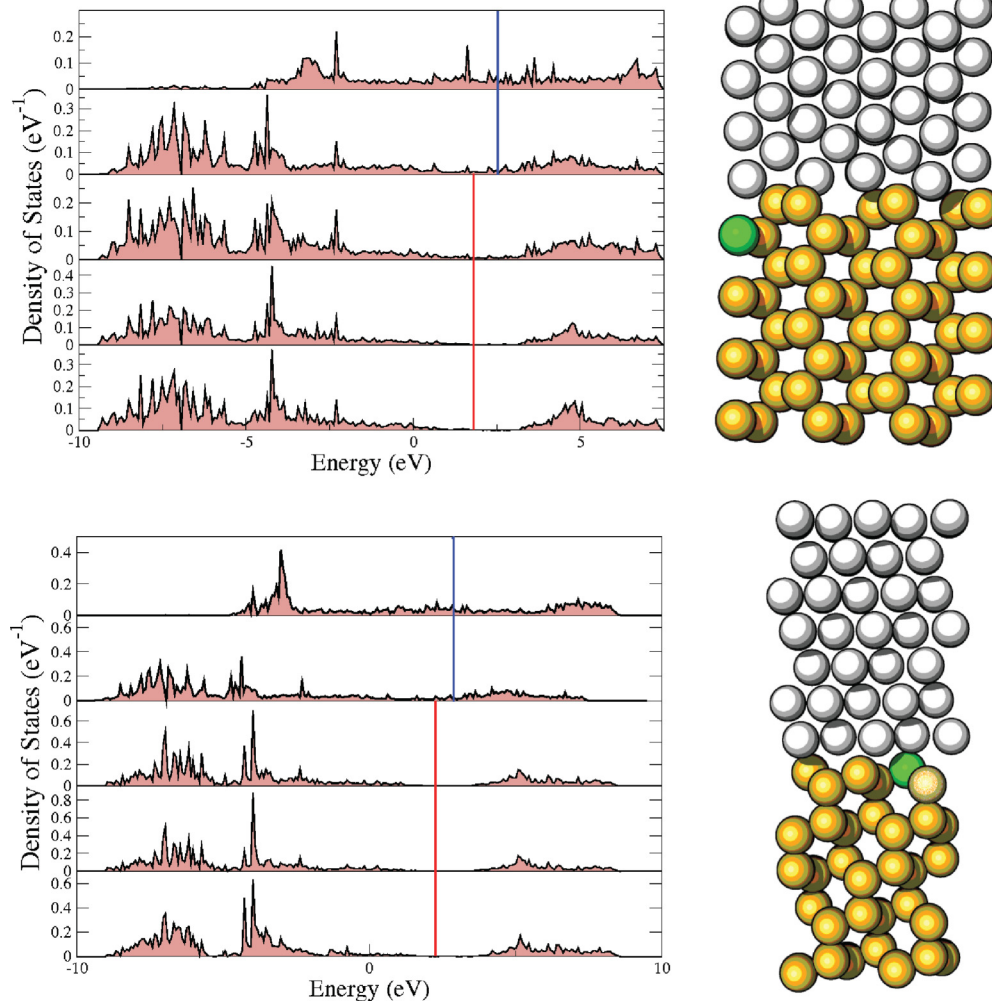


FIG. 7. (Color online) Projected densities of states for the Ag and Si layers closest to the interface. The Ag layers are at the top moving into Si layers towards the bottom. Upper plot is the (110) interface; lower plot is the (111) interface. Interface Fermi levels are highlighted by the blue lines; the Si valence band maxima are represented by the red lines.

TABLE III. Schottky barrier heights (ϕ) for the Si/Ag (110)/(110) and (111)/(111) systems at various doping levels (N_D) as calculated from supercell simulations.

Interface	N_D (cm ⁻³)	ϕ_n (eV)	ϕ_p (eV)
(110)/(110)		0.52	0.58
(110)/(110)	1.73×10^{20}	0.36	0.64
(110)/(110)	1.16×10^{20}	0.37	0.63
(111)/(111)		0.74	0.36
(111)/(111)	2.78×10^{20}	0.52	0.58
(111)/(111)	1.39×10^{20}	0.50	0.60

undoped case the metal-induced gap states (MIGS) decay more quickly in the (111)/(111) interface than in the (110)/(110) interface. In order to calculate the n -SBH we require the difference between the Fermi energy of the interface and the conduction band minimum of the semiconductor. We first calculate the p -SBH as the difference between the valence band maximum (VBM) and the Fermi energy and then calculate the n -SBH by subtracting the p -SBH from the band gap. We use the experimental band gap as GGA DFT methods, such as the PBE functional which we have used, often seriously underestimate the band gap. As can be seen from the PDOS plot in Fig. 7, states in the band gap of the DOS caused by the presence of the metal make the definition of the VBM difficult from these calculations; therefore we calculate the VBM for bulk Si and fit the DOS from the supercell calculations to this through a reference value as in our previous study.⁶ However, in this instance we set the reference state as the core $1s$ energy levels of the bulk Si and the Si atoms far from the interface in the supercell calculations. We believe that this gives a more reliable reference value than the valence band bottom previously used; however, we note that although the SBH for undoped Si/Ag interfaces are altered from our previous study, this alteration is not significant. In both systems the n -SBH is lowered in the presence of P doping (see Table III), as we expected, due to the charge buildup relative to the undoped system. Also, the reduction in the n -SBH is more pronounced in the (111)/(111) system than the (110)/(110) system. This corresponds to the more pronounced charge difference at this interface compared to the (110)/(110) interface.

To investigate the influence of the doping concentration on the change in SBH we have considered both systems at higher levels of doping. The difference between the SBH at the different doping concentrations is not significant, which shows that while the presence of dopant P at the interface has an effect on the SBH, this effect is saturated beyond a certain level of doping. Within the current limits of system size imposed by

the computational demands of such simulations we can say that the effect of dopant P is saturated beyond $\sim 1.2 \times 10^{20}$. In addition we note that the small differences between the SBH in the different sized supercells (≤ 0.2 eV) suggests that the presence of periodic boundaries, which can affect eigenvalue levels, does not affect the accuracy of the calculated SBH in these systems.

VII. CONCLUSIONS

In this paper we have explored the effects of phosphorus doping on the Si/Ag interface as found in high-performance solar cells using first-principles calculations. First we demonstrated how the presence of P doping at the interface increases the stability of this interface. We explained the stabilization relative to the undoped interface by examination of the lattice strain caused by the formation of the interface, showing that strain is reduced in the presence of P. We then related this stabilization of the interface to the experimental observation of increased Ag crystallite formation in the presence of P doping. Using CNT we show how the increased stability of the interfaces results in a higher nucleation rate of crystallites.

We then investigated the effects of P doping on the n -SBH at the two interfaces. We showed, by comparison to the undoped interface, how the presence of P leads to charge buildups at both interfaces, resulting in a net positive charge buildup in the Si wafer and negative buildup in the Ag crystallite. We find that at both interfaces there is a resultant decrease in the SBH in the presence of P doping. The decrease in n -SBH at the (111)/(111) interface is found to be greater, correlating to the greater difference in charge at the interface compared to the undoped interface. The n -SBH calculated in both cases is found to differ significantly (> 100 meV) from the undoped case, suggesting the need to account for doping effects when calculating SBH values for use in device scale models.

ACKNOWLEDGMENTS

The authors acknowledge support from the European Commission grant MMP3-SL-2009-228513, ‘‘Hipersol,’’ as part of the 7th Framework package, Grant No. 228513. Via our membership of the UK’s Materials Chemistry Consortium, which is funded by EPSRC (EP/F067496), this work made use of the facilities of HECToR, the UK’s national high-performance computing service, which is provided by UoE HPCx Ltd. at the University of Edinburgh, Cray Inc., and NAG Ltd., and funded by the Office of Science and Technology through EPSRC’s High End Computing Programme. We also acknowledge the use of supercomputer resources from the Norwegian Notur facility.

¹C. Ballif, D. M. Huljić, G. Willeke, and A. Hessler-Wyser, *Appl. Phys. Lett.* **82**, 1878 (2003).

²Z. G. Li, L. Liang, and L. K. Cheng, *J. Appl. Phys.* **105**, 066102 (2009).

³M. Hörteis, T. Gutberlet, A. Reller, and S. W. Glunz, *Adv. Funct. Mater.* **20**, 476 (2010).

⁴M. M. Hilali, M. M. Al-Jassim, B. To, H. Moutinho, A. Rohatgi, and S. Asher, *J. Electrochem. Soc.* **152**, G742 (2005).

⁵D. Pysch, A. Mette, A. Filipovic, and S. W. Glunz, *Prog. Photovoltaics* **17**, 101 (2009).

⁶K. T. Butler, P. E. Vullum, A. M. Mugggerud, E. Cabrera, and J. H. Harding, *Phys. Rev. B* **83**, 235307 (2011).

⁷C. Ballif, D. Huijic, A. Hessler-Wyser, and G. Willeke, in *Photovoltaic Specialists Conference, 2002. Conference Record of the Twenty-Ninth IEEE* (IEEE, New York, 2002), pp. 360–363.

- ⁸Y.-L. Kuo, J.-J. Huang, S.-T. Lin, C. Lee, and W.-H. Lee, *Mater. Chem. Phys.* **80**, 690 (2003).
- ⁹H.-C. Fang, C.-P. Liu, H.-S. Chung, and C.-L. Huang, *Microsc. Microanal.* **16**, 1340 (2010).
- ¹⁰G. Schubert, Ph.D. thesis, Universitat Konstanz, 2006.
- ¹¹A. Y. C. Yu, *Solid-State Electron.* **13**, 239 (1970).
- ¹²A. M. Cowley and S. M. Sze, *J. Appl. Phys.* **36**, 3212 (1965).
- ¹³W. Schottky, *Z. Phys.* **113**, 367 (1939).
- ¹⁴W. Schottky, *Z. Phys.* **118**, 539 (1942).
- ¹⁵S. G. Louie, J. R. Chelikowsky, and M. L. Cohen, *Phys. Rev. B* **15**, 2154 (1977).
- ¹⁶C. Berthod, N. Binggeli, and A. Baldereschi, *Phys. Rev. B* **68**, 085323 (2003).
- ¹⁷J. R. Waldrop and R. W. Grant, *Appl. Phys. Lett.* **62**, 2685 (1993).
- ¹⁸J. R. Waldrop, *J. Appl. Phys.* **75**, 4548 (1994).
- ¹⁹M. Peressi, N. Binggeli, and A. Baldereschi, *J. Phys. D* **31**, 1273 (1998).
- ²⁰G. Kresse and J. Hafner, *Phys. Rev. B* **49**, 14251 (1994).
- ²¹J. P. Perdew, K. Burke, and M. Ernzerhof, *Phys. Rev. Lett.* **77**, 3865 (1996).
- ²²G. Kresse and D. Joubert, *Phys. Rev. B* **59**, 1758 (1999).
- ²³M. Stutzmann, D. K. Biegelsen, and R. A. Street, *Phys. Rev. B* **35**, 5666 (1987).
- ²⁴J. Robertson, *Phys. Rev. B* **31**, 3817 (1985).
- ²⁵P. Debenedetti (ed.), *Metastable Liquids* (Princeton University Press, Princeton, 1996).
- ²⁶X. Y. Liu and S. W. Lim, *J. Am. Chem. Soc.* **125**, 888 (2002).
- ²⁷M. W. Finnis, *J. Phys.: Condens. Matter* **8**, 5811 (1996).
- ²⁸P. A. Schultz, *Phys. Rev. B* **60**, 1551 (1999).
- ²⁹G. Makov and M. C. Payne, *Phys. Rev. B* **51**, 4014 (1995).
- ³⁰N. D. M. Hine, K. Frensch, W. M. C. Foulkes, and M. W. Finnis, *Phys. Rev. B* **79**, 024112 (2009).
- ³¹J. Lento, J.-L. Mozos, and R. M. Nieminen, *J. Phys.: Condens. Matter* **14**, 2637 (2002).
- ³²S. Angioletti-Uberti, M. Ceriotti, P. D. Lee, and M. W. Finnis, *Phys. Rev. B* **81**, 125416 (2010).
- ³³F. Leroy, D. J. V. A. dos Santos, and F. Müller-Plathe, *Macromol. Rapid Commun.* **30**, 864 (2009).